Kondo phase transitions of magnetic impurities in carbon nanotubes

Tie-Feng Fang[1,2] and Qing-feng Sun[2]
[1]*Center for Interdisciplinary Studies, Lanzhou University, Lanzhou 730000, China*
[2]*Institute of Physics, Chinese Academy of Sciences, Beijing 100080, China*
(Received 9 August 2012; published 13 February 2013)

We propose carbon nanotubes (CNTs) with magnetic impurities as a versatile platform to achieve exciting Kondo physics, where the CNT bath is gapped by the spin-orbit interaction and renormalized by interference effects. While the strong-coupling phase is inaccessible for the special case of half-filled impurities in neutral armchair CNTs, the system in general can undergo quantum phase transitions to the Kondo ground state. The resultant position-specific phase diagrams are investigated upon variation of the CNT radius, chirality, and carrier doping, revealing several striking features, e.g., the existence of a maximal radius for nonarmchair CNTs to realize phase transitions, and an interference-induced suppression of the Kondo screening. We show that by tuning the Fermi energy via electrostatic gating, the quantum critical region can be experimentally accessed.

DOI: 10.1103/PhysRevB.87.075116 PACS number(s): 73.22.−f, 64.70.Tg, 72.15.Qm, 73.20.Hb

I. INTRODUCTION

Carbon nanotubes (CNTs) are formed by wrapping a graphene sheet into a cylinder of nanometer radius.[1] Their exceptional electronic structure has allowed the exploration of various fascinating Kondo phenomena, including the singlet-triplet Kondo resonance,[2] the enhanced shot noise[3] due to the SU(4) Kondo effect,[4] and the competitions with ferromagnetism[5] as well as superconductivity.[6] These studies have utilized short CNTs to construct quantum dots behaving as artificial magnetic impurities. Long CNTs, on the other hand, can play the role of one-dimensional host for a real magnetic impurity, which may be either a magnetic adatom on the top of a carbon atom (T site) or at the center of a hexagon (C site), or a substitutional dopant in a carbon vacancy (S site). Indeed, Kondo physics for cobalt clusters adsorbed on metallic CNTs has already been observed.[7] This has spurred several theoretical works[8–10] to address related issues. However, a generic Kondo model of a CNT-hosted magnetic impurity, pertaining to arbitrary positions at the atomic scale, has not yet been established. More importantly, while these theories[8–10] have all considered the metallic-CNT host as a one-dimensional normal metal with a constant density of states (DOS) near the Fermi energy to produce the Kondo effect,[11] recent experiments[12] and calculations[13–15] have demonstrated that metallic CNTs cannot be normal metal, always having rich low-energy band structures due to the spin-orbit interaction (SOI) and surface curvature. Interesting Kondo physics then arises when these ingredients in the CNT host are included.

In this paper, after establishing a generic Hamiltonian for magnetic impurities in metallic CNTs, we show that, depending on explicit impurity positions, the system can be mapped onto two kinds of Kondo models whose host DOS are identically gapped by the SOI and curvature effect but scale distinctly outside the gap region due to the absence (for T sites) and presence (for S or C sites) of quantum interference between different hybridization paths. We combine renormalization group (RG) arguments and slave boson (SB) techniques to demonstrate that the local-moment (LM) state persists for half-filled impurities in neutral armchair CNTs due to the particle-hole (p-h) symmetry. Away from this special case, quantum phase transitions (QPTs) exist in these gapped systems, separating the Kondo and LM ground states. The resultant phase diagrams are characterized by the CNT radius, chirality, carrier doping, and the impurity positions. The effect of quantum interference is found to reduce the Kondo regime, making S and C configurations unfavorable for Kondo screening as compared with T sites. For sufficiently deep impurity levels, two quantum critical regions are accessible by scanning tunneling probes and gating the CNT host, with signatures characterizing the nonarmchair from armchair chiralities for small-radius CNTs.

II. MODEL HAMILTONIAN

Our starting point is the Anderson Hamiltonian of a magnetic impurity in graphene, $\mathcal{H}=\mathcal{H}_o+\mathcal{H}_g+\mathcal{H}_{og}$, where $\mathcal{H}_o=\sum_\sigma \varepsilon_d d_\sigma^\dagger d_\sigma+\frac{U}{2}\sum_\sigma d_\sigma^\dagger d_\sigma d_{\bar\sigma}^\dagger d_{\bar\sigma}$ models the impurity, as usual.[11] $\mathcal{H}_g$ is the graphene tight-binding Hamiltonian reading $\mathcal{H}_g=\sum_{\langle i,j\rangle,\sigma} t a_\sigma^\dagger(\mathbf{R}_{ai})b_\sigma(\mathbf{R}_{bj})+\text{H.c.}$; here $a_\sigma(\mathbf{R}_{ai})$ $[b_\sigma(\mathbf{R}_{bj})]$ annihilates a π-band electron on sublattice A (B) at position $\mathbf{R}_{ai}$ $(\mathbf{R}_{bj})$, and t is the nearest-neighbor hopping energy. The hybridization term $\mathcal{H}_{og}=\sum_\sigma g_\sigma^\dagger d_\sigma+\text{H.c.}$ with $g_\sigma^\dagger=\sum_{\langle j\rangle}[V_{aj}a_\sigma^\dagger(\mathbf{R}_{aj})+V_{bj}b_\sigma^\dagger(\mathbf{R}_{bj})]$, where $\langle j\rangle$ stands for the A and/or B sublattice sites nearest to the impurity and V_{xj} $(x=a,b)$ represent the corresponding hybridization amplitudes. In particular, $g_\sigma^\dagger=V_{a1}a_\sigma^\dagger(0)$ for a T-site adatom. C-site impurities can hybridize with six surrounding carbon atoms, yielding $g_\sigma^\dagger=\sum_{j=1}^3[V_{aj}a_\sigma^\dagger(\mathbf{X}_j)+V_{bj}b_\sigma^\dagger(-\mathbf{X}_j)]$ with $\mathbf{X}_j$ being the lattice nearest-neighbor vectors, while $g_\sigma^\dagger=\sum_{j=1}^3 V_{bj}b_\sigma^\dagger(\mathbf{X}_j)$ for S-site impurities on sublattice A. In momentum space, the fermionic basis $c_{\mathbf{k}\sigma\alpha}\equiv\frac{1}{\sqrt{2}}(\alpha a_{\mathbf{k}\sigma}+\frac{\phi_{\mathbf{k}}}{|\phi_{\mathbf{k}}|}b_{\mathbf{k}\sigma})$ diagonalizes the graphene Hamiltonian as $\mathcal{H}_g=\sum_{\mathbf{k},\sigma,\alpha}\varepsilon_\alpha(\mathbf{k})c_{\mathbf{k}\sigma\alpha}^\dagger c_{\mathbf{k}\sigma\alpha}$, where $\phi_{\mathbf{k}}=\sum_{j=1}^3 e^{i\mathbf{k}\cdot\mathbf{X}_j}$, $\varepsilon_\alpha(\mathbf{k})=\alpha t|\phi_{\mathbf{k}}|$, and $\alpha=\pm1$. Close to the Dirac points $\mathbf{K}$, the dispersion is linear, i.e., $\varepsilon_\alpha(\mathbf{K}+\boldsymbol{\kappa})\simeq\alpha\hbar v_F|\boldsymbol{\kappa}|$ for $|\boldsymbol{\kappa}|\ll|\mathbf{K}|$, with v_F being the Fermi velocity. In this basis, the hybridization becomes $\mathcal{H}_{og}=\sum_{\mathbf{k},\sigma,\alpha}V_\alpha(\mathbf{k})c_{\mathbf{k}\sigma\alpha}^\dagger d_\sigma+\text{H.c.}$, where $V_\alpha(\mathbf{k})=(\alpha\Phi_{a\mathbf{k}}+\Phi_{b\mathbf{k}}|\phi_{\mathbf{k}}|/\phi_{\mathbf{k}}^*)/\sqrt{2N}$, with $\Phi_{x\mathbf{k}}=\sum_{\langle j\rangle}V_{xj}e^{-i\mathbf{k}\cdot\mathbf{R}_{xj}}$ and N being the number of sublattice sites.

We now roll up the graphene sheet along the chiral vector $\mathbf{C}_h = n_1\mathbf{a}_1 + n_2\mathbf{a}_2$ to create a (n_1, n_2) CNT,[1] where $n_1, n_2 \in \mathbb{Z}$ and $\mathbf{a}_1, \mathbf{a}_2$ are the primitive lattice vectors. While the $\boldsymbol{\kappa}$ component parallel to the tube axis, $p \equiv \kappa_\parallel$, remains continuous for CNTs of long length L, the periodic boundary condition, $(\mathbf{K} + \boldsymbol{\kappa}) \cdot \mathbf{C}_h = 2\pi m$, $m \in \mathbb{Z}$, quantizes $\boldsymbol{\kappa}$'s perpendicular component, $q_\tau \equiv \kappa_\perp = \frac{\tau\nu}{3R}$ for the lowest π subband. Here $R = \frac{a}{2\pi}(n_1^2 + n_2^2 + n_1 n_2)^{1/2}$ is the tube radius with $a = |\mathbf{a}_1| \simeq 2.46$ Å being the lattice constant, the valley index $\tau = \pm 1$ denotes the two inequivalent $\mathbf{K}^+$, $\mathbf{K}^-$ Dirac points, and $\nu = \mathrm{mod}(n_1 - n_2, 3)$. Restricting the graphene quantities, $\varepsilon_\alpha(\mathbf{k})$, $V_\alpha(\mathbf{k})$, $c_{\mathbf{k}\sigma\alpha}$, only to these allowed Bloch states near the Dirac points yields corresponding quantities for the CNT: the π-band spectrum $\varepsilon_{p\tau\alpha} = \alpha\hbar v_F (p^2 + q_\tau^2)^{1/2}$, the hybridization $V_{p\tau\alpha} = V_\alpha(\mathbf{K}^\tau + \boldsymbol{\kappa})|_{\boldsymbol{\kappa}=(p,\, q_\tau)}$, and the operator $c_{p\sigma\tau\alpha}$.

The surface curvature of CNTs induces the π band hybridizing with other high-energy bands and enhances the effect of intrinsic SOI, V_{so}, of carbon atoms. At second order in perturbation theory based on a double expansion of V_{so} and a/R,[14,15] the SOI gives a spin-dependent shift $\frac{\sigma\alpha_1 V_{\mathrm{so}} a}{\hbar v_F R}$ of q_τ and directly shifts the energy dispersion by $-\sigma\tau\alpha_2 V_{\mathrm{so}}(a/R)\cos 3\theta$, while the curvature-induced hybridization only causes a valley-dependent q_τ shift $\frac{\tau\beta a^2 \cos 3\theta}{\hbar v_F R^2}$. Here α_1, α_2, β are unperturbed parameters (see Appendix A for their expressions and values), the spin $\sigma = \pm$, and θ is the angle between the chiral vector and the zigzag direction along $\mathbf{a}_1$, calculated by $\theta = \arctan\frac{\sqrt{3}n_2}{2n_1 + n_2}$ for $0 \leqslant n_2 \leqslant n_1$. These corrections result in $q_\tau \to q_{\sigma\tau} = \frac{\tau\Delta_{\mathrm{cv}}}{\hbar v_F} + \frac{\sigma\Delta_{\mathrm{so1}}}{\hbar v_F}$ for metallic CNTs ($\nu = 0$), $\varepsilon_{p\tau\alpha} \to \varepsilon_{p\sigma\tau\alpha} = \alpha\hbar v_F (p^2 + q_{\sigma\tau}^2)^{1/2} - \sigma\tau\Delta_{\mathrm{so2}}$, and $V_{p\tau\alpha} \to V_{p\sigma\tau\alpha} = V_\alpha(\mathbf{K}^\tau + \boldsymbol{\kappa})|_{\boldsymbol{\kappa}=(p,\, q_{\sigma\tau})}$, by setting $\Delta_{\mathrm{so1}} = \alpha_1 V_{\mathrm{so}} a/R$, $\Delta_{\mathrm{so2}} = \alpha_2 V_{\mathrm{so}}(a/R)\cos 3\theta$, and $\Delta_{\mathrm{cv}} = \beta(a/R)^2 \cos 3\theta$. The CNT spectrum $\varepsilon_{p\sigma\tau\alpha}$ derived here is in agreement with existed band-structure calculations.[13–15] Our generic Anderson Hamiltonian for a magnetic impurity coupled to the metallic CNT host then reads $\mathcal{H} = \mathcal{H}_o + \mathcal{H}_c$,

$$\mathcal{H}_c = \sum_{p,\sigma,\tau,\alpha} [\varepsilon_{p\sigma\tau\alpha} c^\dagger_{p\sigma\tau\alpha} c_{p\sigma\tau\alpha} + (V_{p\sigma\tau\alpha} c^\dagger_{p\sigma\tau\alpha} d_\sigma + \mathrm{H.c.})], \tag{1}$$

with the host DOS, $\rho_{\sigma\tau}(\varepsilon) \equiv \sum_{p,\alpha} \delta(\varepsilon - \varepsilon_{p\sigma\tau\alpha})$, given by

$$\rho_{\sigma\tau}(\varepsilon) = \rho_0 \frac{|\varepsilon + \sigma\tau\Delta_{\mathrm{so2}}|\, \Theta(|\varepsilon + \sigma\tau\Delta_{\mathrm{so2}}| - \Delta_{\sigma\tau})}{\sqrt{(\varepsilon + \sigma\tau\Delta_{\mathrm{so2}})^2 - \Delta_{\sigma\tau}^2}}, \tag{2}$$

where $\rho_0 = L/(h v_F)$ and $\Delta_{\sigma\tau} = |\Delta_{\mathrm{cv}} + \sigma\tau\Delta_{\mathrm{so1}}|$. Note that a gap of width $2\Delta_{\sigma\tau}$ opens even in metallic CNTs, with integrable singularities at the gap edges.

Impurity physics is fully determined by the hybridization function,[16] $\Gamma(\varepsilon) = \pi \sum_{p,\tau,\alpha} |V_{p\sigma\tau\alpha}|^2 \delta(\varepsilon - \varepsilon_{p\sigma\tau\alpha})$, which must be spin independent due to the nonmagnetic nature of the CNT. This allows us to replace $V_{p\sigma\tau\alpha}$ and $\varepsilon_{p\sigma\tau\alpha}$ in Eq. (1) by a proper constant coupling V_0 and an effective spectrum $\widetilde{\varepsilon}_p$, as long as $\widetilde{\varepsilon}_p$ is defined such that its effective DOS $\widetilde{\rho}(\varepsilon) \equiv \sum_{p,\tau,\alpha} \delta(\varepsilon - \widetilde{\varepsilon}_p)$ equals $\Gamma(\varepsilon)/(\pi V_0^2)$, i.e., the hybridization function remains unchanged. By applying the Schrieffer-Wolff transformation,[17] the system can then be readily mapped onto the Kondo model $\mathcal{H}_K = J\hat{\mathbf{S}} \cdot \hat{\mathbf{s}}$ which describes the exchange interaction $J = -2V_0^2 U/[\widetilde{\varepsilon}_d(\widetilde{\varepsilon}_d + U)] > 0$ of the impurity spin $\hat{\mathbf{S}}$ with the host spin $\hat{\mathbf{s}}$, where $\widetilde{\varepsilon}_d = \varepsilon_d - E_F < 0$ is the impurity level relative to the Fermi energy E_F. Details of the transformation are in Appendix B.

The effective DOS $\widetilde{\rho}(\varepsilon)$ is essentially a renormalization of the bare CNT DOS, emerging from the quantum interference between different paths the impurity can take to hybridize with the host. By ignoring this interference and also the SOI, Ref. 10 suggests that impurities adsorbed inside the CNT are much more hybridized, resulting in large V_0 and thus large Kondo temperatures. The Jahn-Teller effect for endohedral impurities can, on the contrary, reduce the hybridization constant to suppress the Kondo effect.[8] Instead of these Kondo phenomena caused by changes in V_0, our work will focus on the effects of SOI and interference, both manifested in the energy dependence of $\widetilde{\rho}(\varepsilon)$. We thus consider a particular class of impurity orbitals that hybridizes equally with the nearest carbon atoms on a given sublattice, i.e., $V_{xj} = V_x$. In this case, when the impurity is located on the S or C site, constructive interference renormalizes the CNT DOS as $\widetilde{\rho}_{\mathrm{sc}}(\varepsilon) = \sum_\tau (\varepsilon + \sigma\tau\Delta_{\mathrm{so2}})^2 \rho_{\sigma\tau}(\varepsilon)/(2Nt^2)$ by defining $V_0 = V_b$ for S sites or $V_0 = (V_a^2 + V_b^2)^{1/2}$ for C sites, whereas $\widetilde{\rho}_{\mathrm{T}}(\varepsilon) = \sum_\tau \rho_{\sigma\tau}(\varepsilon)/(2N)$ for T-site adatoms where $V_0 = V_a$ and the interference is absent. These DOS, with corresponding figures given in Appendix C, represent two distinct classes of gapped Kondo models promising for exciting Kondo physics.

III. RENORMALIZATION-GROUP SCALING AND SLAVE-BOSON MEAN-FIELD THEORY

(i) A half-filled ($U = -2\widetilde{\varepsilon}_d$) impurity coupled to the neutral armchair ($\theta = 30^\circ$) CNT where, since $\Delta_{\mathrm{so2}} = \Delta_{\mathrm{cv}} = 0$, the curvature-induced hybridization is absent and the SOI opens a gap of width $2\Delta_{\mathrm{so1}}$ at the Fermi level that exactly crosses the Dirac point. The system then exhibits strict p-h symmetry. Its ground state is determined by the RG scaling for the Anderson instead of the Kondo Hamiltonian because the former contains relevant degrees of freedom.[18] After integrating out high-energy states with energy $\pm\Lambda$ in the band edges, the RG scaling gives a beta function of the localized level $\beta(\widetilde{\varepsilon}_d)$ in which all even powers of $\widetilde{\varepsilon}_d$ are eliminated by p-h symmetry.[11] Up to the leading order in V_0 and $\widetilde{\varepsilon}_d$, which arises from two-loop vertex renormalizations, one has $\beta(\widetilde{\varepsilon}_d) = 4\widetilde{\rho}(\Lambda)V_0^2\widetilde{\varepsilon}_d/\Lambda$. Consequently, the flow of the Kondo coupling $J = -4V_0^2/\widetilde{\varepsilon}_d$ reads $\beta(J) = -4\widetilde{\rho}(\Lambda)V_0^2 J/\Lambda$. Solving this RG equation yields $J(\Lambda) = J(\Lambda_0)\exp\{-4V_0^2 \int_{\Lambda_0}^{\Lambda} [\widetilde{\rho}(\Lambda)/\Lambda^2] d\Lambda\}$, where Λ_0 is the initial band cutoff. As the scaling of the gapped impurity model characterized by $\widetilde{\rho}_{\mathrm{sc}}(\varepsilon)$ or $\widetilde{\rho}_{\mathrm{T}}(\varepsilon)$ terminates at the gap edge $\Lambda = \Delta_{\mathrm{so1}}$, $J(\Lambda)$ flows to a finite value rather than infinity, signaling the absence of the strong-coupling Kondo phase. Therefore, the impurity ground state is always a local moment, consistent with previous numerical RG calculations on the rectangularly gapped band.[19]

(ii) An infinite-U impurity in the neutral armchair CNT. Here, p-h symmetry of the impurity is maximally violated giving $J = -2V_0^2/\widetilde{\varepsilon}_d$, whereas the CNT bath remains p-h symmetric. RG transformations of the Kondo Hamiltonian can then be applied. As conduction states in the band edges are integrated out, J is renormalized as $J \to J + \widetilde{\rho}(\Lambda)J^2\delta\Lambda/\Lambda$ to leading one-loop order,[11,20] so that the RG scaling equation

of dimensionless Kondo coupling $\widetilde{J} \equiv \widetilde{\rho}(\Lambda)J$ reads $\beta(\widetilde{J}) = [\ln \widetilde{\rho}(\Lambda)]'_\Lambda \widetilde{J} - \widetilde{J}^2$. We solve the beta function as

$$\widetilde{J}(\Lambda) = \frac{\widetilde{\rho}(\Lambda)\widetilde{J}(\Lambda_0)}{\widetilde{\rho}(\Lambda_0) + \widetilde{J}(\Lambda_0)\int_{\Lambda_0}^{\Lambda}[\widetilde{\rho}(\Lambda)/\Lambda]\,d\Lambda}, \tag{3}$$

where the denominator being vanishing or nonvanishing during scaling determines the impurity ground state.

For T-site adatoms, the DOS is $\widetilde{\rho}_{\rm T}(\varepsilon) = \widetilde{\rho}_0\Theta(|\varepsilon| - \Delta_{\rm so1})|\varepsilon|/(\varepsilon^2 - \Delta_{\rm so1}^2)^{1/2}$ with $\widetilde{\rho}_0 \equiv \frac{\rho_0}{N}$. As the scaling proceeds, the denominator of Eq. (3) vanishes at the critical band width $\Lambda_c = T_{\rm K}^0 + \Delta_{\rm so1}^2/(4T_{\rm K}^0)$ when $2T_{\rm K}^0 > \Delta_{\rm so1}$, directing the RG flow towards the strong-coupling Kondo fixed point. Here the Kondo temperature $T_{\rm K}^0 \equiv \Lambda_0 \exp[-1/\widetilde{J}(\Lambda_0)]$ is defined as a scaling invariant[11] of the normal metallic model [realized by setting $\widetilde{\rho}(\varepsilon) = \widetilde{\rho}_{\rm T}(\Lambda_0) \simeq \widetilde{\rho}_0$ for $\Lambda_0 \gg \Delta_{\rm so1}$]. By contrast, for $2T_{\rm K}^0 < \Delta_{\rm so1}$, or equivalently, $\widetilde{J}(\Lambda_0) < [\ln(2\Lambda_0/\Delta_{\rm so1})]^{-1}$, the adatom flows to the unscreened LM state since the coupling $\widetilde{J}(\Lambda)$ already vanishes as the scaling enters into the gap region before it reaches the strong-coupling limit. We thus find a quantum critical point of the impurity level $\widetilde{\varepsilon}_{dc} = -2V_0^2\widetilde{\rho}_0 \ln\frac{2\Lambda_0}{\Delta_{\rm so1}}$ across which, upon lowering $\widetilde{\varepsilon}_d$, the impurity undergoes a QPT from a screened to an unscreened moment. The explicit R dependence of this phase boundary can be written as $\widetilde{\varepsilon}_{dc} = \varepsilon_{c1} - 2V_0^2\widetilde{\rho}_0 \ln\frac{R}{a}$, with $\varepsilon_{c1} = -2V_0^2\widetilde{\rho}_0 \ln\frac{2\Lambda_0}{\alpha_1 V_{\rm so}}$. As compared to the previously numerical RG-studied DOS with a rectangular gap,[19] $\widetilde{\rho}_0\Theta(|\varepsilon| - \Delta)$, whose phase boundary is determined by $T_{\rm K}^0 = \Delta$, it is clear that the Kondo regime in the present case expands significantly due to the divergent but integrable DOS at gap edges.

The interference-induced additional scaling $(\varepsilon/t)^2$ imposed on the effective host DOS $\widetilde{\rho}_{\rm sc}(\varepsilon) = (\varepsilon/t)^2\widetilde{\rho}_{\rm T}(\varepsilon)$ for substitutional dopants or C-site adatoms dramatically changes the RG flow of Eq. (3). It features a different phase boundary at $\widetilde{\varepsilon}_{dc} = \varepsilon_{c2} - f(\frac{R}{a})$ separating the Kondo and LM phases, where $\varepsilon_{c2} = -V_0^2\widetilde{\rho}_0\frac{\Lambda_0^2}{t^2}$ and

$$f\left(\frac{R}{a}\right) = V_0^2\widetilde{\rho}_0\frac{\alpha_1^2V_{\rm so}^2a^2}{t^2R^2}\ln\frac{2\Lambda_0R}{\alpha_1V_{\rm so}a},$$

by taking $\widetilde{\rho}_{\rm sc}(\Lambda_0) \simeq \widetilde{\rho}_0\frac{\Lambda_0^2}{t^2}$ for $\Lambda_0 \gg \Delta_{\rm so1}$. For realistic parameters, this boundary is always much shallower than in the T-site case, reflecting a reduction of the Kondo regime by the interference.

(iii) An infinite-U impurity in the carrier-doped nanotube with arbitrary chirality. In this case, Eq. (2) shows that the gaps for the two valleys are different, being centered at $\pm\Delta_{\rm so2}$ with width $W_1 = 2|\Delta_{\rm cv} - \Delta_{\rm so1}|$ and $W_2 = 2(\Delta_{\rm cv} + \Delta_{\rm so1})$, respectively. Summing over the two valleys, their overlap constitutes a net gap of width $W = (W_1 + W_2)/2 - 2\Delta_{\rm so2}$ centered at $\varepsilon_0 \equiv \min(\Delta_{\rm cv}, \Delta_{\rm so1})$, in the effective DOS $\widetilde{\rho}_{\rm T}(\varepsilon)$ and $\widetilde{\rho}_{\rm sc}(\varepsilon)$.

That $\Delta_{\rm so2}$ and $\Delta_{\rm cv}$ are nonzero for nonarmchair chiralities, and the deviation of the Fermi level from the Dirac point in doped CNTs, definitely break the p-h symmetry of the bath DOS. This renders the previous RG arguments invalid because all vertex functions will develop structures. The SB mean-field theory[21] accounts for this complication by introducing an auxiliary boson field that is further condensed to its saddle-point value r. At criticality, the Kondo temperature $T_{\rm K}$ must vanish. The saddle-point equations then yield the critical value of the impurity level,

$$\widetilde{\varepsilon}_{dc} = \frac{1}{\pi}\int_{-\Lambda_0}^{E_F} d\varepsilon\frac{\Gamma(\varepsilon)}{\varepsilon - E_F} + \frac{1}{\pi}\int_{E_F}^{\Lambda_0} d\varepsilon\frac{\Gamma(\varepsilon)}{E_F - \varepsilon}, \tag{4}$$

with full details presented in Appendix D. Besides confirming the same critical values derived in situation (ii), Eq. (4) is indeed applicable to carrier-doped and nonarmchair CNTs. Below we present numerical results for realistic CNT parameters:[14] $\alpha_1 = 0.055$, $\alpha_2 = 0.217$, $\beta = 93.75$ meV, $V_{\rm so} = 6$ meV, and $t = 2.5$ eV.

IV. NUMERICAL RESULTS AND DISCUSSIONS

Figure 1 presents impurity phase diagrams in the $(\widetilde{\varepsilon}_d, R)$ plane, when the Fermi energy is tuned to the gap center, $E_F = \varepsilon_0$. The QPTs discussed here exist only if the CNT bath is gapped, such that $\widetilde{\rho}(E_F)$ vanishes exactly. Solving the inequality $W > 0$, we find a critical chiral angle $\theta_0 = \frac{1}{3}\arccos(\alpha_1/\alpha_2) \approx 25.1^\circ$ and an upper limit of CNT radius $R_0 = \beta a/(V_{\rm so}\alpha_2) \approx 17.7$ nm. For $\theta_0 < \theta \leqslant 30^\circ$, CNTs with arbitrary radius are always gapped ($W > 0$), resulting in the impurity exhibiting Kondo and LM ground states separated by transitions at $\widetilde{\varepsilon}_{dc}$ in the whole range of R [see, e.g., Figs. 1(a) and 1(b) for the armchair case]. On the other hand, when $0 \leqslant \theta \leqslant \theta_0$, the Kondo-LM transition can occur only for $R < R_0$. Beyond this upper limit $R \geqslant R_0$, one has $W \leqslant 0$, leaving always a screened impurity state [see, e.g., Figs. 1(c) and 1(d) for the zigzag case]. The specific R dependence of the phase boundary is also very sensitive to explicit impurity positions, despite $\widetilde{\rho}_{\rm T}(\varepsilon)$ and $\widetilde{\rho}_{\rm sc}(\varepsilon)$ featuring the same gap structure. When the CNT radius increases so that the gap width decreases, the Kondo regime of impurities on T (S or C) sites gradually widens (narrows), with the boundary eventually decreasing to $-\infty$ (increasing to ε_{c2}) as $R \to \infty$ for $\theta > \theta_0$ chiralities [see, e.g., Figs. 1(a) and 1(b)] and $R \to R_0$ for $\theta \leqslant \theta_0$ chiralities [see, e.g., Figs. 1(c) and 1(d)].

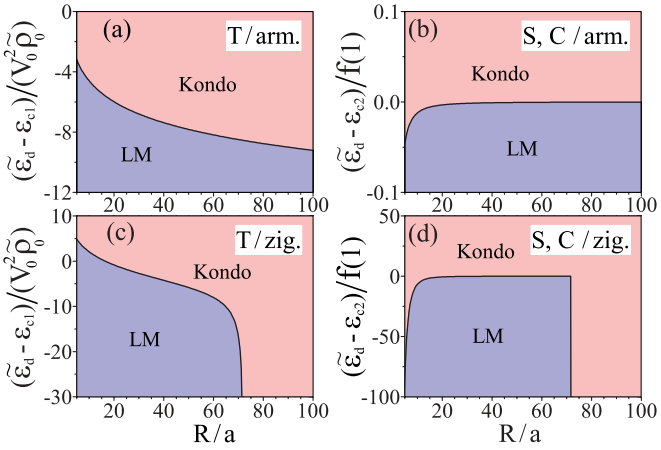

FIG. 1. (Color online) Phase diagrams of Kondo-LM transitions for impurities sitting on T [(a), (c)], S or C [(b), (d)] sites in the (n,n) armchair [(a), (b)] and $(3n,0)$ zigzag [(c), (d)] CNTs, as a function of the impurity level $\widetilde{\varepsilon}_d$ and discrete CNT radius $R/a = \sqrt{3}n/(2\pi)$ (armchair), $3n/(2\pi)$ (zigzag), with $n \in \mathbb{Z}$. The high-energy cutoff $\Lambda_0 = 0.5$ eV.

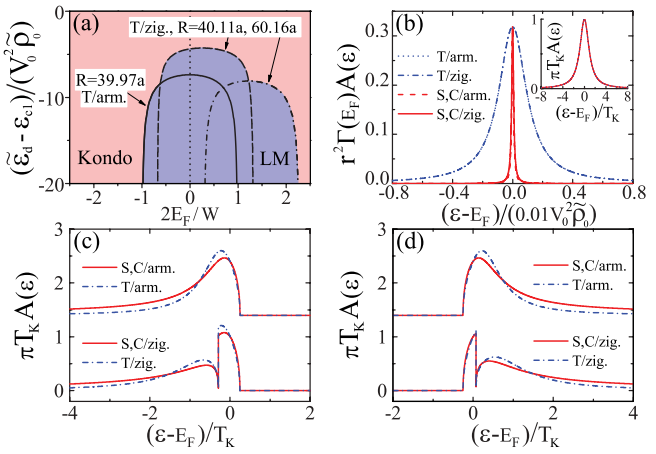

FIG. 2. (Color online) (a) Phase diagrams for T-site adatoms upon variation of the Fermi energy E_F, with $\Lambda_0 = 0.5$ eV. (b)–(d) Spectral density of a deep impurity level $\widetilde{\varepsilon}_d = -25V_0^2\widetilde{\rho}_0$ in (20,20) armchair and (36, 0) zigzag CNTs with comparable radii, for $E_F - \varepsilon_0 = -0.88t$ (b), $-0.55W$ (c), and $0.55W$ (d), with $\Lambda_0 = t$. In panels (c) and (d), we set $V_0^2 = 0.1W/[\pi r^2\widetilde{\rho}(E_F)]$ such that $T_K \simeq 0.1W \simeq 0.01$ meV (armchair), 0.5 meV (zigzag), and curves regarding armchair CNTs are offset for clarity.

This sensitiveness stems from the quantum interference effect, which dramatically changes the scaling behavior of $\widetilde{\rho}_{SC}(\varepsilon)$ outside the gap region, as compared with $\widetilde{\rho}_T(\varepsilon)$. By noting $\varepsilon_{c1} \simeq 400\varepsilon_{c2} \simeq -10^8 f(1) < 0$ for the parameters used here, an interference-induced overall shrinking of the Kondo regime in the S and C configurations is also evident, as already stated.

Gating the CNT host to tune its Fermi energy away from the gap center renders E_F closer to electronic states near one of the gap edges, in favor of screening the impurity. Therefore, the strong-coupling fixed point can be reached for smaller Kondo couplings (deeper impurity levels), widening the Kondo regime. This is confirmed by our calculations shown in Fig. 2(a) for T-site adatoms (the corresponding figure for S- or C-site impurities is given in Appendix E), where the Kondo and LM phases are bounded by an arched borderline peaked at $E_F = \varepsilon_0$. As E_F moves farther out of the gap region, arbitrary small $J > 0$ can always drive the impurity into the Kondo phase due to $\widetilde{\rho}(E_F) \neq 0$. Interestingly, while the armchair CNT features a p-h symmetric phase diagram when it is tuned from hole doping ($E_F < 0$) to electron doping ($E_F > 0$), the arched phase boundary of nonarmchair CNTs always deviates from the hole-doped side because of $\varepsilon_0 > 0$ and can even fully enter into the electron-doped region for large CNT radius. The minimal radius R_1 needed for accessing this maximal p-h asymmetry can be determined by solving $\varepsilon_0 > \frac{W}{2}$ to obtain $R_1 = R_0 \frac{\alpha_2 \cos 3\theta}{\alpha_1 + \alpha_2 \cos 3\theta}$ when $\theta \leqslant \theta_0$, thereby $R_1 \approx 14.1$ nm for zigzag CNTs.

Obviously, for deep impurity levels, two consecutive QPTs occur whenever the Fermi energy sweeps over the two gap edges. These can be experimentally observed via scanning tunneling probes[7] which directly measure the impurity spectral density $A(\varepsilon)$ calculated by the SB technique (see Appendix D for details). By placing the Fermi energy far away from the gap region [Fig. 2(b)], the smooth host DOS around E_F gives rise to conventional Kondo resonances in $A(\varepsilon)$. While the CNT chiralities are indistinguishable in these resonances, the interference inbuilt in the S and C configurations greatly narrows the resonances as compared with T sites, signaling a suppression of the Kondo effect which is not favorable for experimental observations, regardless of the existing universal scaling with the Kondo temperature [inset of Fig. 2(b)]. This scaling is violated when E_F is tuned to access the quantum critical region around the gap edges [Figs. 2(c) and 2(d)]. Specifically, although the scaling of different impurity positions persists to some extent, the zigzag CNT hosts two-peak Kondo resonances distinct from the armchair one. We attribute this two-peak signature to a distortion by the characteristic DOS of small-radius nonarmchair CNTs, which possesses two singularities near each gap edge arising from the two nondegenerate valleys. Finally, as E_F shifts into the gap region, the SB equations break down and the Kondo resonances immediately collapse into featureless LM spectra.

V. CONCLUSIONS

In conclusion, we have addressed the Kondo problem of magnetic impurities in CNTs, demonstrating the existence of distinct QPTs in the impurity ground state, which crucially depends on the characteristics of CNT and explicit impurity positions.

ACKNOWLEDGMENTS

T.-F. Fang is grateful to A.-M. Guo and H.-W. Liu for inspiring discussions. This work is financially supported by NBRP of China (2012CB921303 and 2009CB929100) and NSF-China.

APPENDIX A: PARAMETERS α_1, α_2, AND β

In the low-energy theory for carbon nanotubes, the effects of spin-orbit interaction and surface curvature on π electrons are well described in second-order perturbation theory.[14,15] The effects are equivalent to shifting the dispersion relation by $-\sigma\tau\alpha_2 V_{so}(a/R)\cos 3\theta$, to shifting the perpendicular wave vector by $\sigma\alpha_1 \frac{V_{so}a}{\hbar v_F R} + \tau\beta \frac{a^2 \cos 3\theta}{\hbar v_F R^2}$, and to shifting the parallel wave vector by $\tau\beta' \frac{a^2 \sin 3\theta}{\hbar v_F R^2}$. Assuming sufficiently long nanotubes, the last shift is irrelevant; we thus drop it. The parameters, α_1, α_2, and β appearing in the remaining terms are related to some unperturbed hopping amplitudes between carbon orbitals. Their explicit forms are[14]

$$\alpha_1 = -\frac{\sqrt{3}\varepsilon_s\left(V_{pp}^{\pi} + V_{pp}^{\sigma}\right)}{18V_{sp}^2}, \tag{A1}$$

$$\alpha_2 = \frac{\sqrt{3}V_{pp}^{\pi}}{3\left(V_{pp}^{\pi} - V_{pp}^{\sigma}\right)}, \tag{A2}$$

$$\beta = \frac{V_{pp}^{\pi}\left(V_{pp}^{\pi} + V_{pp}^{\sigma}\right)}{8\left(V_{pp}^{\pi} - V_{pp}^{\sigma}\right)}. \tag{A3}$$

Here ε_s is the energy of the carbon s orbital relative to the p orbital energy. The latter (i.e., the on-site energy of π electrons) is set to zero in our paper. V_{sp} represents the unperturbed hopping amplitude between nearest-neighbor s and p orbitals. $V_{pp}^{\pi(\sigma)}$ is the unperturbed hopping amplitude

between nearest-neighbor p orbitals, giving rise to the π (σ) band. In this work, we use the parameter set[22] $\varepsilon_s = -8.9$ eV, $V_{sp} = 5.6$ eV, $V_{pp}^{\pi} = -3.0$ eV, and $V_{pp}^{\sigma} = 5.0$ eV as also used in Ref. 14. This gives us $\alpha_1 \simeq 0.055$, $\alpha_2 \simeq 0.217$, and $\beta \simeq 93.75$ meV, to carry out numerical calculations. Using other sets of parameters, e.g., Ref. 23, does not change our numerical results qualitatively.

APPENDIX B: SCHRIEFFER-WOLFF TRANSFORMATION

The Schrieffer-Wolff transformation establishes the relation between the Anderson and Kondo models. While the original work of Schrieffer and Wolff[17] used a canonical transformation to derive the Kondo Hamiltonian from the Anderson Hamiltonian, here we adopt a more straightforward method, i.e., the projection method,[11] for this purpose. We start from the generic Anderson model for an adatom in the nanotube after the replacement of $\varepsilon_{p\sigma\tau\alpha}$ and $V_{p\sigma\tau\alpha}$ by $\widetilde{\varepsilon}_p$ and V_0, which reads ($\sigma = \uparrow, \downarrow$)

$$\mathcal{H} = \varepsilon_d \hat{n} + U \hat{n}_\uparrow \hat{n}_\downarrow + \sum_{p,\sigma,\tau,\alpha} \widetilde{\varepsilon}_p c^\dagger_{p\sigma\tau\alpha} c_{p\sigma\tau\alpha} + \sum_{p,\sigma,\tau,\alpha} (V_0 c^\dagger_{p\sigma\tau\alpha} d_\sigma + V_0 d^\dagger_\sigma c_{p\sigma\tau\alpha}), \tag{B1}$$

where $\hat{n} = \hat{n}_\uparrow + \hat{n}_\downarrow$ with $\hat{n}_\sigma = d^\dagger_\sigma d_\sigma$. One should bear in mind that, depending on the nanotube characteristics, the effective CNT spectrum, $\widetilde{\rho}(\varepsilon) = \sum_{p,\tau,\alpha} \delta(\varepsilon - \widetilde{\varepsilon}_p)$, is energy dependent and can be gapped around the Fermi level E_F.

The whole Hilbert space of Eq. (B1) can be projected into three subspaces where the impurity state is empty ($n = 0$), singly occupied ($n = 1$), and doubly occupied ($n = 2$), respectively, by using the projection operators

$$\hat{P}_0 = 1 - \hat{n} + \hat{n}_\uparrow \hat{n}_\downarrow, \tag{B2}$$

$$\hat{P}_1 = \hat{n} - 2\hat{n}_\uparrow \hat{n}_\downarrow, \tag{B3}$$

$$\hat{P}_2 = \hat{n}_\uparrow \hat{n}_\downarrow. \tag{B4}$$

Accordingly, the components of the total wave function Ψ in the three subspaces are denoted by ψ_0, ψ_1, and ψ_2, respectively. Then the Schrödinger equation $\mathcal{H}\Psi = E\Psi$ can be expressed in the form

$$\begin{pmatrix} \mathcal{H}_{00} & \mathcal{H}_{01} & \mathcal{H}_{02} \\ \mathcal{H}_{10} & \mathcal{H}_{11} & \mathcal{H}_{12} \\ \mathcal{H}_{20} & \mathcal{H}_{21} & \mathcal{H}_{22} \end{pmatrix} \begin{pmatrix} \psi_0 \\ \psi_1 \\ \psi_2 \end{pmatrix} = E \begin{pmatrix} \psi_0 \\ \psi_1 \\ \psi_2 \end{pmatrix}, \tag{B5}$$

where $\mathcal{H}_{nn'} = \hat{P}_n \mathcal{H} \hat{P}_{n'}$. These matrix elements are

$$\mathcal{H}_{00} = \sum_{p,\sigma,\tau,\alpha} \widetilde{\varepsilon}_p \hat{P}_0 c^\dagger_{p\sigma\tau\alpha} c_{p\sigma\tau\alpha}, \tag{B6}$$

$$\mathcal{H}_{11} = \varepsilon_d \hat{P}_1 + \sum_{p,\sigma,\tau,\alpha} \widetilde{\varepsilon}_p \hat{P}_1 c^\dagger_{p\sigma\tau\alpha} c_{p\sigma\tau\alpha}, \tag{B7}$$

$$\mathcal{H}_{22} = (2\varepsilon_d + U)\, \hat{P}_2 + \sum_{p,\sigma,\tau,\alpha} \widetilde{\varepsilon}_p \hat{P}_2 c^\dagger_{p\sigma\tau\alpha} c_{p\sigma\tau\alpha}, \tag{B8}$$

$$\mathcal{H}_{10} = \mathcal{H}^\dagger_{01} = \sum_{p,\sigma,\tau,\alpha} V_0 d^\dagger_\sigma (1 - \hat{n}_{\bar{\sigma}})\, c_{p\sigma\tau\alpha}, \tag{B9}$$

$$\mathcal{H}_{21} = \mathcal{H}^\dagger_{12} = \sum_{p,\sigma,\tau,\alpha} V_0 d^\dagger_\sigma \hat{n}_{\bar{\sigma}} c_{p\sigma\tau\alpha}, \tag{B10}$$

$$\mathcal{H}_{20} = \mathcal{H}^\dagger_{02} = 0. \tag{B11}$$

By eliminating ψ_0 and ψ_2 from Eq. (B5), one obtains the effective Schrödinger equation, $\mathcal{H}_{\rm eff}\psi_1 = E\psi_1$, in the singly occupied subspace, with the effective Hamiltonian given by

$$\mathcal{H}_{\rm eff} = \mathcal{H}_{11} + \mathcal{H}_{12}\,(E - \mathcal{H}_{22})^{-1}\,\mathcal{H}_{21} + \mathcal{H}_{10}\,(E - \mathcal{H}_{00})^{-1}\,\mathcal{H}_{01}. \tag{B12}$$

The first term on the right-hand side of Eq. (B12) is the energy of the singly occupied subspace when $V_0 = 0$. The second term describes the energy arising from the mixing of the singly occupied and doubly occupied subspaces due to $V_0 \neq 0$, and the third term is for the mixing of the singly occupied and empty subspaces. So far, no approximation has been used and the effective Hamiltonian Eq. (B12) is exact.

For the parameter regime in which the ground-state configuration of the Anderson model for $V_0 = 0$ is the singly occupied one, the doubly occupied and empty configurations are higher excited states. The effects of virtual excitations from the singly occupied state to these excited states can be taken into account to lowest order in V_0 by replacing $E - \mathcal{H}_{22}$ with $E_1 - E_2$ and replacing $E - \mathcal{H}_{00}$ with $E_1 - E_0$ in Eq. (B12). E_0, E_1, and E_2 are respectively the energies for the empty, singly, and doubly occupied states when $V_0 = 0$. Under this approximation, the second term in Eq. (B12) becomes

$$\begin{aligned} \mathcal{H}_{12}\,(E - \mathcal{H}_{22})^{-1}\,\mathcal{H}_{21} \approx \mathcal{H}_{12}\,(E_1 - E_2)^{-1}\,\mathcal{H}_{21} &= \sum_{p,\sigma,\tau,\alpha} \sum_{p',\sigma',\tau',\alpha'} \frac{V_0^2}{\widetilde{\varepsilon}_{p'} - \varepsilon_d - U} c^\dagger_{p\sigma\tau\alpha} c_{p'\sigma'\tau'\alpha'} d_\sigma \hat{n}_{\bar{\sigma}} d^\dagger_{\sigma'} \hat{n}_{\bar{\sigma}'} \\ &= \sum_{p,\tau,\alpha} \sum_{p',\tau',\alpha'} \frac{V_0^2}{\varepsilon_d + U - \widetilde{\varepsilon}_{p'}} [\hat{S}^z (c^\dagger_{p\uparrow\tau\alpha} c_{p'\uparrow\tau'\alpha'} - c^\dagger_{p\downarrow\tau\alpha} c_{p'\downarrow\tau'\alpha'}) + \hat{S}^+ c^\dagger_{p\downarrow\tau\alpha} c_{p'\uparrow\tau'\alpha'} + \hat{S}^- c^\dagger_{p\uparrow\tau\alpha} c_{p'\downarrow\tau'\alpha'}] \\ &\quad + \frac{1}{2} \sum_{p,\sigma,\tau,\alpha} \sum_{p',\tau',\alpha'} \frac{V_0^2}{\widetilde{\varepsilon}_{p'} - \varepsilon_d - U} c^\dagger_{p\sigma\tau\alpha} c_{p'\sigma\tau'\alpha'} (\hat{n} - 2\hat{n}_\downarrow \hat{n}_\uparrow), \end{aligned} \tag{B13}$$

where we have introduced the spin operators for the impurity:

$$\hat{S}^z = \tfrac{1}{2}(\hat{n}_\uparrow - \hat{n}_\downarrow), \tag{B14}$$

$$\hat{S}^+ = d^\dagger_\uparrow d_\downarrow, \tag{B15}$$

$$\hat{S}^- = d^\dagger_\downarrow d_\uparrow. \tag{B16}$$

The third term in Eq. (B12) becomes

$$\mathcal{H}_{10}(E-\mathcal{H}_{00})^{-1}\mathcal{H}_{01} \approx \mathcal{H}_{10}(E_1-E_0)^{-1}\mathcal{H}_{01} = \sum_{p,\sigma,\tau,\alpha}\sum_{p',\sigma',\tau',\alpha'}\frac{V_0^2}{\varepsilon_d-\widetilde{\varepsilon}_p}c_{p'\sigma'\tau'\alpha'}c^\dagger_{p\sigma\tau\alpha}d^\dagger_{\sigma'}(1-\hat{n}_{\overline{\sigma'}})(1-\hat{n}_{\overline{\sigma}})d_\sigma$$

$$= \mathcal{H}_b + \sum_{p,\sigma,\tau,\alpha}\sum_{p',\sigma',\tau',\alpha'}\frac{V_0^2}{\widetilde{\varepsilon}_p-\varepsilon_d}c^\dagger_{p\sigma\tau\alpha}c_{p'\sigma'\tau'\alpha'}d^\dagger_{\sigma'}(1-\hat{n}_{\overline{\sigma'}})(1-\hat{n}_{\overline{\sigma}})d_\sigma$$

$$= \mathcal{H}_b + \sum_{p,\tau,\alpha}\sum_{p',\tau',\alpha'}\frac{V_0^2}{\widetilde{\varepsilon}_p-\varepsilon_d}[\hat{S}^z(c^\dagger_{p\uparrow\tau\alpha}c_{p'\uparrow\tau'\alpha'}-c^\dagger_{p\downarrow\tau\alpha}c_{p'\downarrow\tau'\alpha'})+\hat{S}^+c^\dagger_{p\downarrow\tau\alpha}c_{p'\uparrow\tau'\alpha'}+\hat{S}^-c^\dagger_{p\uparrow\tau\alpha}c_{p'\downarrow\tau'\alpha'}]$$

$$+\frac{1}{2}\sum_{p,\sigma,\tau,\alpha}\sum_{p',\tau',\alpha'}\frac{V_0^2}{\widetilde{\varepsilon}_p-\varepsilon_d}c^\dagger_{p\sigma\tau\alpha}c_{p'\sigma\tau'\alpha'}(\hat{n}-2\hat{n}_\uparrow\hat{n}_\downarrow), \tag{B17}$$

where

$$\mathcal{H}_b = \sum_{p,\sigma,\tau,\alpha}\frac{V_0^2}{\varepsilon_d-\widetilde{\varepsilon}_p}(\hat{n}_\sigma-\hat{n}_\uparrow\hat{n}_\downarrow) = \int_{-\Lambda_0}^{\Lambda_0}d\varepsilon\frac{V_0^2\widetilde{\rho}(\varepsilon)}{\varepsilon_d-\varepsilon}(\hat{n}-2\hat{n}_\uparrow\hat{n}_\downarrow). \tag{B18}$$

Substituting Eqs. (B7), (B13), and (B17) into Eq. (B12), the effective Hamiltonian reads

$$\mathcal{H}_{\rm eff} = \left[\varepsilon_d+\int_{-\Lambda_0}^{\Lambda_0}d\varepsilon\frac{V_0^2\widetilde{\rho}(\varepsilon)}{\varepsilon_d-\varepsilon}\right](\hat{n}-2\hat{n}_\uparrow\hat{n}_\downarrow)+\sum_{p,\sigma,\tau,\alpha}\widetilde{\varepsilon}_pc^\dagger_{p\sigma\tau\alpha}c_{p\sigma\tau\alpha}(\hat{n}-2\hat{n}_\uparrow\hat{n}_\downarrow)$$

$$+\frac{1}{2}\sum_{p,\sigma,\tau,\alpha}\sum_{p',\tau',\alpha'}\left(\frac{V_0^2}{\widetilde{\varepsilon}_p-\varepsilon_d}-\frac{V_0^2}{\varepsilon_d+U-\widetilde{\varepsilon}_{p'}}\right)c^\dagger_{p\sigma\tau\alpha}c_{p'\sigma\tau'\alpha'}(\hat{n}-2\hat{n}_\uparrow\hat{n}_\downarrow) \tag{B19}$$

$$+\frac{1}{2}\sum_{p,\tau,\alpha}\sum_{p',\tau',\alpha'}\left(\frac{2V_0^2}{\widetilde{\varepsilon}_p-\varepsilon_d}+\frac{2V_0^2}{\varepsilon_d+U-\widetilde{\varepsilon}_{p'}}\right)[\hat{S}^z(c^\dagger_{p\uparrow\tau\alpha}c_{p'\uparrow\tau'\alpha'}-c^\dagger_{p\downarrow\tau\alpha}c_{p'\downarrow\tau'\alpha'})+\hat{S}^+c^\dagger_{p\downarrow\tau\alpha}c_{p'\uparrow\tau'\alpha'}+\hat{S}^-c^\dagger_{p\uparrow\tau\alpha}c_{p'\downarrow\tau'\alpha'}].$$

Equation (B19) is valid in the local moment limit where the impurity state is singly occupied and its charge fluctuations are frozen out. In this regime, the relations $\hat{n}=1$ and $\hat{n}_\uparrow\hat{n}_\downarrow=0$ hold. Therefore, the first term on the right-hand side of Eq. (B19) becomes a constant. The second term is the Hamiltonian for conduction electrons in the nanotube bath. The third term describes the trivial potential scattering of conduction electrons. The last term gives the *s*-*d* Kondo model with the exchange interaction given by

$$J_{pp'} = \frac{2V_0^2}{\widetilde{\varepsilon}_p-\varepsilon_d}+\frac{2V_0^2}{\varepsilon_d+U-\widetilde{\varepsilon}_{p'}}. \tag{B20}$$

We emphasize here that in the above derivations of the exchange coupling $J_{pp'}$, no any assumption about the CNT bath has been made. Eq. (B20) is applicable to arbitrary CNT spectrum of $\widetilde{\rho}(\varepsilon)$, no matter if $\widetilde{\rho}(\varepsilon)$ is constant or energy-dependent, smooth or gapped.

The local-moment limit is realized for the impurity parameter $\varepsilon_d < E_F$ and $\varepsilon_d+U > E_F$. In this case, when the nanotube bath is not gapped or the gap does not cross the Fermi level, the conduction electrons being exchange scattered by the impurity spin are near the Fermi level and the exchange scattering is elastic. We can thus approximate $\widetilde{\varepsilon}_p, \widetilde{\varepsilon}_{p'} \approx E_F$ in Eq. (B20) to obtain a constant exchange interaction $J = 2V_0^2U/[(\varepsilon_d-E_F)(E_F-\varepsilon_d-U)]$. When the Fermi level lies within the gap, the situation becomes a bit complex due to the absence of electronic states at E_F. In such a case, the exchange-scattered conduction electrons are near the two gap edges, and the scattering may be inelastic, suffering an energy change equal to the gap width. For example, an electron at the lower gap edge can be scattered into the upper edge. This indicates that $\widetilde{\varepsilon}_p, \widetilde{\varepsilon}_{p'}$ in Eq. (B20) should be approximated by $\varepsilon_{\rm up}$ and/or $\varepsilon_{\rm low}$, rather than E_F; here $\varepsilon_{\rm up}$ and $\varepsilon_{\rm low}$ denote the energies of the upper and lower gap edges, respectively. However, for a sufficiently deep impurity level, a sufficiently large Coulomb repulsion, and a sufficiently small gap width, i.e., in the parameter regime of

$$E_F-\varepsilon_d \gg |E_F-\varepsilon_{\rm up(low)}|, \quad \varepsilon_d+U-E_F \gg |E_F-\varepsilon_{\rm up(low)}|, \tag{B21}$$

the approximation $\widetilde{\varepsilon}_p, \widetilde{\varepsilon}_{p'} \approx E_F$ is still valid. In this paper, all our results, presented for the Fermi level lying within the gap, fall into this parameter regime. Therefore, no matter the nanotube bath is gapped or not gapped and the Fermi level is inside or outside the gap, we always obtain the Kondo model

$$\mathcal{H}_K = \frac{1}{2}J\sum_{p,\tau,\alpha}\sum_{p',\tau',\alpha'}[S^z(c^\dagger_{p\uparrow\tau\alpha}c_{p'\uparrow\tau'\alpha'}-c^\dagger_{p\downarrow\tau\alpha}c_{p'\downarrow\tau'\alpha'})$$

$$+S^+c^\dagger_{p\downarrow\tau\alpha}c_{p'\uparrow\tau'\alpha'}+S^-c^\dagger_{p\uparrow\tau\alpha}c_{p'\downarrow\tau'\alpha'}], \tag{B22}$$

with a constant antiferromagnetic exchange interaction $J > 0$.

Introducing the Pauli matrices

$$\hat{\sigma}^z = \begin{pmatrix}1 & 0\\ 0 & -1\end{pmatrix}, \quad \hat{\sigma}^+ = \begin{pmatrix}0 & 2\\ 0 & 0\end{pmatrix}, \quad \hat{\sigma}^- = \begin{pmatrix}0 & 0\\ 2 & 0\end{pmatrix}, \tag{B23}$$

and using the relation for the vectors of impurity spin operators $\hat{\mathbf{S}}$ and Pauli matrices $\hat{\boldsymbol{\sigma}}$

$$\hat{\mathbf{S}}\cdot\hat{\boldsymbol{\sigma}} = \hat{S}^z\hat{\sigma}^z+\tfrac{1}{2}\hat{S}^+\hat{\sigma}^-+\tfrac{1}{2}\hat{S}^-\hat{\sigma}^+, \tag{B24}$$

the Kondo model Eq. (B22) can be rewritten as

$$\mathcal{H}_K = \frac{1}{2} J \sum_{p,\sigma,\tau,\alpha} \sum_{p',\sigma',\tau',\alpha'} \hat{\mathbf{S}} \cdot \hat{\boldsymbol{\sigma}}_{\sigma\sigma'} c^{\dagger}_{p\sigma\tau\alpha} c_{p'\sigma'\tau'\alpha'} = J \hat{\mathbf{S}} \cdot \hat{\mathbf{s}}, \tag{B25}$$

where $\hat{\mathbf{s}} = \frac{1}{2} \sum_{p,\sigma,\tau,\alpha} \sum_{p',\sigma',\tau',\alpha'} \hat{\boldsymbol{\sigma}}_{\sigma\sigma'} c^{\dagger}_{p\sigma\tau\alpha} c_{p'\sigma'\tau'\alpha'}$ is defined as the spin of conduction electrons at the impurity site.

APPENDIX C: BAND STRUCTURE, BARE DOS, AND EFFECTIVE DOS OF CARBON NANOTUBES WITH SPIN-ORBIT INTERACTION AND CURVATURE EFFECT

The low-energy band structure of nanotubes calculated from the spectrum $\varepsilon_{p\sigma\tau\alpha}$, the bare nanotube DOS $\rho_{\sigma\tau}(\varepsilon)$, the DOS $\widetilde{\rho}_{\mathrm{T}}(\varepsilon)$ felt by T-site adatoms, and the effective DOS $\widetilde{\rho}_{\mathrm{SC}}(\varepsilon)$ renormalized by the interference effect for S- or C-site impurities are all presented in Fig. 3. For armchair nanotubes [Figs. 3(a), 3(e), 3(i), and 3(m)], the band and DOS are symmetric, having a gap centered at the Dirac point. Even if the radius of armchair nanotubes varies, the qualitative features of these line shapes will always remain the same. Only the gap width will change because it is inversely proportional to the radius, $W = 2\Delta_{\mathrm{so1}} \propto \frac{1}{R}$. However, this is not the case for zigzag nanotubes, whose asymmetric band structure and DOS can dramatically evolve upon variation of the radius, as shown in Figs. 3(b)–3(d), 3(f)–3(h), 3(j)–3(l), and 3(n)–3(p). In particular, the gap of zigzag nanotubes is jointly determined by Δ_{so1}, Δ_{so2}, and Δ_{cv}. Both the gap width and position evolve with the tube radius. In the case of $R < R_1$ [Figs. 3(b), 3(f), 3(j), and 3(n)], the gap asymmetrically crosses the Dirac point, with the gap center always on the high-energy side of the Dirac point. For $R_1 < R < R_0$ [Figs. 3(c), 3(g), 3(k), and 3(o)], the entire gap region lies above the Dirac point, giving rise to the maximal p-h asymmetry of phase diagrams in the $(\widetilde{\varepsilon}_d, E_F)$ plane [see Figs. 2(a) and 5]. Finally, no gap exists in zigzag nanotubes when $R > R_0$ [Figs. 3(d), 3(h), 3(l), and 3(p)], leaving always a Kondo-screened impurity without phase transition to the local-moment state [see Figs. 1(c) and 1(d)]. It is evident in Figs. 3(i)–3(p) that the interference effect inbuilt in S and C configurations qualitatively alters the scaling behavior of the nanotube DOS as compared with T-site adatoms, although the gap structure remains the same.

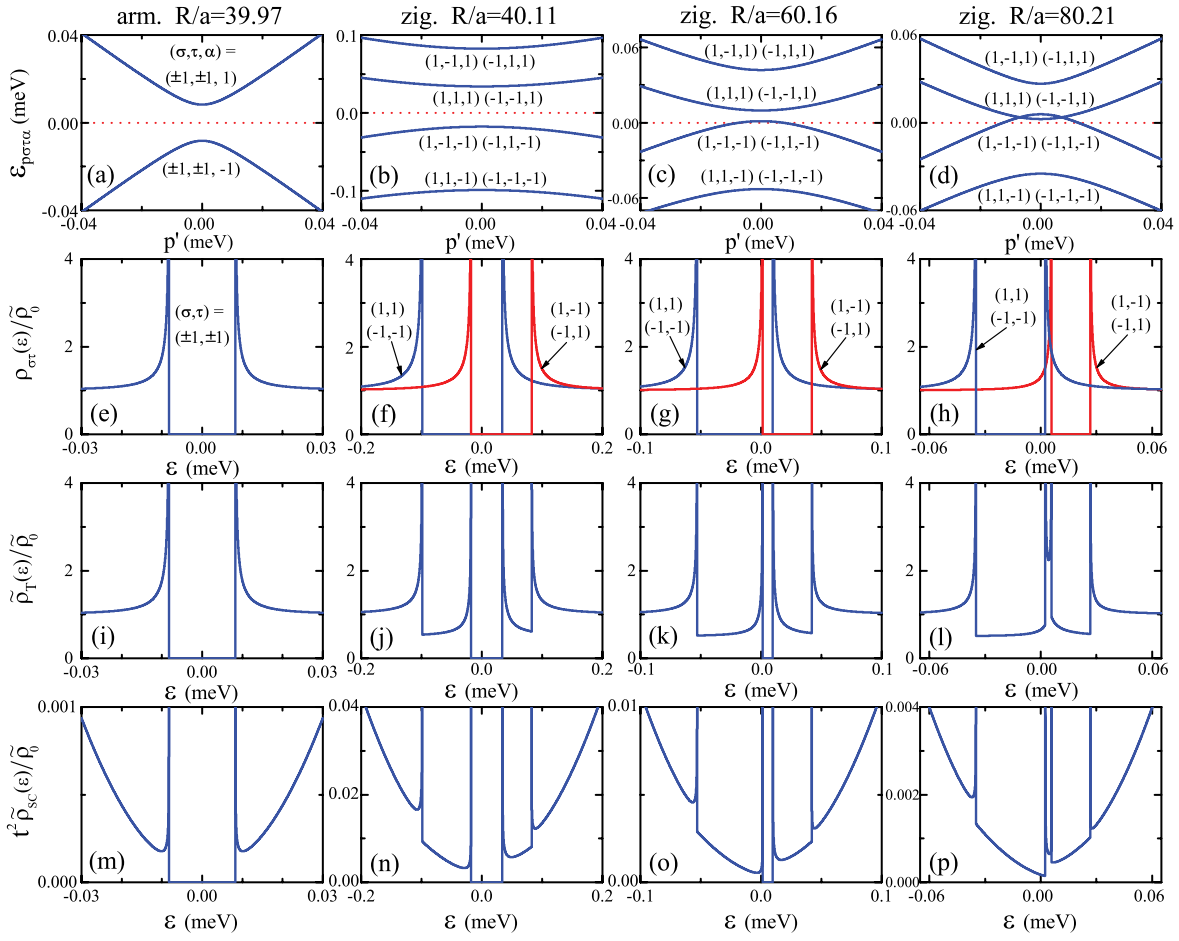

FIG. 3. (Color online) (a)–(d) Nanotube band structure $\varepsilon_{p\sigma\tau\alpha}$ as a function of the momentum $p' \equiv \hbar v_F p$, the dotted lines denote the position of Dirac point. (e)–(h) Bare nanotube DOS $\rho_{\sigma\tau}(\varepsilon)$ as a function of energy. (i)–(l) the DOS $\widetilde{\rho}_{\mathrm{T}}(\varepsilon)$ felt by T-site adatoms. (m)–(p) the effective DOS $\widetilde{\rho}_{\mathrm{SC}}(\varepsilon)$ renormalized by the interference effect for S- and C-site impurities. The first column [(a), (e), (i), and (m)] is for an armchair nanotube with the radius $R = 39.97a$. The second column [(b), (f), (j), and (n)] is for a zigzag nanotube with the radius $R = 40.11a < R_1$. The third column [(c), (g), (k), and (o)] is for a zigzag nanotube with the radius $R = 60.16a$, a value satisfying $R_1 < R < R_0$. The last column [(d), (h), (l), and (p)] is for a zigzag nanotube with the radius $R = 80.21a > R_0$. The definitions of R_0 and R_1 are presented in the main text.

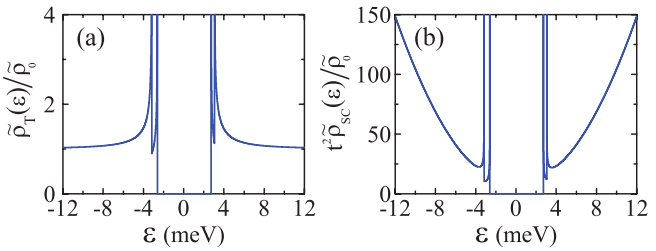

FIG. 4. (Color online) DOS of a (36, 0) zigzag nanotube whose radius is $R \simeq 5.7a$, for impurities at T sites (a) and S/C sites (b).

Another significant difference between the armchair- and zigzag-nanotube DOS is that, while the former always has only one singularity at each gap edge, the latter possesses two singularities on each side of the gap [see Figs. 3(i)–3(k) and 3(m)–3(o)]. For small-radius zigzag nanotubes, e.g., a (36, 0) nanotube with the radius $R \simeq 5.7a$, the distance d between the two singularities on the same side of the gap becomes far, far smaller than the gap width W, as shown in Fig. 4. The condition $T_K \sim d \ll W$ can thus be fulfilled near the quantum critical region. In this case, the two singularities can produce a signature of nonarmchair chiralities in the critical Kondo resonance, which is discussed in the main text [see Figs. 2(c) and 2(d)].

APPENDIX D: SLAVE-BOSON MEAN-FIELD THEORY

For $U \to \infty$, double occupancy of the impurity state is forbidden. Our generic Anderson Hamiltonian for carbon nanotubes with an adsorbed impurity may be written in the slave-boson representation,

$$\mathcal{H}_{SB} = \sum_{p,\sigma,\tau,\alpha} \varepsilon_{p\sigma\tau\alpha} c^\dagger_{p\sigma\tau\alpha} c_{p\sigma\tau\alpha} + \sum_\sigma \varepsilon_d f^\dagger_\sigma f_\sigma + \sum_{p,\sigma,\tau,\alpha} (V_{p\sigma\tau\alpha} c^\dagger_{p\sigma\tau\alpha} b^\dagger f_\sigma + \text{H.c.}) + \lambda\left(b^\dagger b + \sum_\sigma f^\dagger_\sigma f_\sigma - 1\right), \tag{D1}$$

where the original impurity operator has been decomposed as $d_\sigma \to b^\dagger f_\sigma$ ($d^\dagger_\sigma \to f^\dagger_\sigma b$). The pseudofermion operator f_σ annihilates the singly occupied state and the auxiliary boson operator $b^\dagger$ creates an empty state. In Eq. (D1), a Lagrange multiplier λ is also introduced to enforce the constraint, $b^\dagger b + \sum_\sigma f^\dagger_\sigma f_\sigma = 1$, as required by the $U \to \infty$ limit. We solve the Hamiltonian within the mean-field approach, which is the leading order in a $1/N$ expansion. This approach sets the boson operator $b^\dagger$ (b) to a classical, nonfluctuating value r, thereby neglecting charge fluctuations. The slave-boson mean-field Hamiltonian is then given by

$$\mathcal{H}_{SBMF} = \sum_{p,\sigma,\tau,\alpha} \varepsilon_{p\sigma\tau\alpha} c^\dagger_{p\sigma\tau\alpha} c_{p\sigma\tau\alpha} + \sum_\sigma (\varepsilon_d + \lambda) f^\dagger_\sigma f_\sigma + \sum_{p,\sigma,\tau,\alpha} (r V_{p\sigma\tau\alpha} c^\dagger_{p\sigma\tau\alpha} f_\sigma + \text{H.c.}) + \lambda(r^2 - 1), \tag{D2}$$

where the two mean-field parameters r and λ have to be determined through their saddle-point equations which minimize the free energy $F \equiv -k_B T \ln[\text{Tr}(e^{-\mathcal{H}_{SBMF}/(k_B T)})]$, i.e.,

$$\frac{\partial F}{\partial r} = 0, \quad \frac{\partial F}{\partial \lambda} = 0. \tag{D3}$$

After some calculations, Eq. (D3) yields

$$\sum_{p,\sigma,\tau,\alpha} [V_{p\sigma\tau\alpha} \langle c^\dagger_{p\sigma\tau\alpha} f_\sigma\rangle + V^*_{p\sigma\tau\alpha} \langle f^\dagger_\sigma c_{p\sigma\tau\alpha}\rangle] + 2\lambda r = 0, \tag{D4}$$

$$r^2 + \sum_\sigma \langle f^\dagger_\sigma f_\sigma\rangle - 1 = 0. \tag{D5}$$

By using the fluctuation-dissipation theorem,

$$\langle \hat{B}\hat{A}\rangle = \frac{i}{2\pi} \int_{-\Lambda_0}^{E_F} d\varepsilon [\langle\langle \hat{A}|\hat{B}\rangle\rangle_{re} - \langle\langle \hat{A}|\hat{B}\rangle\rangle_{ad}], \tag{D6}$$

the equilibrium thermal averages in Eqs. (D4) and (D5) are related to the corresponding retarded $\langle\langle\cdot|\cdot\rangle\rangle_{re}$ and advanced $\langle\langle\cdot|\cdot\rangle\rangle_{ad}$ Green functions. We thus obtain

$$\frac{i}{2\pi} \int_{-\Lambda_0}^{E_F} d\varepsilon \sum_{p,\sigma,\tau,\alpha} \begin{bmatrix} V_{p\sigma\tau\alpha} \langle\langle f_\sigma | c^\dagger_{p\sigma\tau\alpha}\rangle\rangle_{re} + V^*_{p\sigma\tau\alpha} \langle\langle c_{p\sigma\tau\alpha} | f^\dagger_\sigma\rangle\rangle_{re} \\ -V_{p\sigma\tau\alpha} \langle\langle f_\sigma | c^\dagger_{p\sigma\tau\alpha}\rangle\rangle_{ad} - V^*_{p\sigma\tau\alpha} \langle\langle c_{p\sigma\tau\alpha} | f^\dagger_\sigma\rangle\rangle_{ad} \end{bmatrix} = -2\lambda r, \tag{D7}$$

$$\frac{i}{2\pi} \int_{-\Lambda_0}^{E_F} d\varepsilon \sum_\sigma [\langle\langle f_\sigma | f^\dagger_\sigma\rangle\rangle_{re} - \langle\langle f_\sigma | f^\dagger_\sigma\rangle\rangle_{ad}] = 1 - r^2. \tag{D8}$$

In order to calculate the Green functions appearing in Eqs. (D7) and (D8), we need to write down their equations of motion in two alternative forms:

$$z\langle\langle \hat{A}|\hat{B}\rangle\rangle = \langle[\hat{A},\hat{B}]_+\rangle + \langle\langle[\hat{A},\ \mathcal{H}_{SBMF}]|\hat{B}\rangle\rangle, \tag{D9}$$

$$z\langle\langle \hat{A}|\hat{B}\rangle\rangle = \langle[\hat{A},\hat{B}]_+\rangle - \langle\langle \hat{A}|[\hat{B},\ \mathcal{H}_{SBMF}]\rangle\rangle, \tag{D10}$$

with $z = \varepsilon + i0^+$ for retarded Green functions and $z = \varepsilon - i0^+$ for advanced ones. Since the mean-field Hamiltonian (D2) is quadratic, having no interacting terms, the involved equations of motion can be readily closed. After some algebra, we obtain exact solutions of these Green functions:

$$\langle\langle f_\sigma | f^\dagger_\sigma\rangle\rangle_{re} = \frac{1}{\varepsilon - (\varepsilon_d + \lambda) - r^2\Sigma(\varepsilon) + i0^+} \equiv G(\varepsilon), \tag{D11}$$

$$\langle\langle f_\sigma | f^\dagger_\sigma\rangle\rangle_{ad} = (\langle\langle f_\sigma | f^\dagger_\sigma\rangle\rangle_{re})^*, \tag{D12}$$

$$\langle\langle c_{p\sigma\tau\alpha} | f^\dagger_\sigma\rangle\rangle_{re} = \frac{r V_{p\sigma\tau\alpha}}{\varepsilon - \varepsilon_{p\sigma\tau\alpha} + i0^+} \langle\langle f_\sigma | f^\dagger_\sigma\rangle\rangle_{re}, \tag{D13}$$

$$\langle\langle c_{p\sigma\tau\alpha}|f_\sigma^\dagger\rangle\rangle_{\rm ad} = \frac{rV_{p\sigma\tau\alpha}}{\varepsilon-\varepsilon_{p\sigma\tau\alpha}-i0^+}\langle\langle f_\sigma|f_\sigma^\dagger\rangle\rangle_{\rm ad}, \quad \text{(D14)}$$

$$\langle\langle f_\sigma|c_{p\sigma\tau\alpha}^\dagger\rangle\rangle_{\rm re} = \frac{rV_{p\sigma\tau\alpha}^*}{\varepsilon-\varepsilon_{p\sigma\tau\alpha}+i0^+}\langle\langle f_\sigma|f_\sigma^\dagger\rangle\rangle_{\rm re}, \quad \text{(D15)}$$

$$\langle\langle f_\sigma|c_{p\sigma\tau\alpha}^\dagger\rangle\rangle_{\rm ad} = \frac{rV_{p\sigma\tau\alpha}^*}{\varepsilon-\varepsilon_{p\sigma\tau\alpha}-i0^+}\langle\langle f_\sigma|f_\sigma^\dagger\rangle\rangle_{\rm ad}, \quad \text{(D16)}$$

with

$$\Sigma(\varepsilon) = \frac{1}{\pi}\int_{-\Lambda_0}^{\Lambda_0} d\varepsilon' \frac{\Gamma(\varepsilon')}{\varepsilon-\varepsilon'+i0^+}, \quad \text{(D17)}$$

the self-energy arising from the hybridization, where $\Gamma(\varepsilon) = \pi\sum_{p,\tau,\alpha}|V_{p\sigma\tau\alpha}|^2\delta(\varepsilon-\varepsilon_{p\sigma\tau\alpha}) = \pi V_0^2\widetilde{\rho}(\varepsilon)$ is the so-called hybridization function which must be spin-independent after summing over the valley states due to the nonmagnetic nature of the nanotube bath. Substituting these solutions into Eqs. (D7) and (D8), the two saddle-point equations finally become

$$\frac{2}{\pi}\int_{-\Lambda_0}^{E_F} d\varepsilon\,{\rm Im}\left[\Sigma(\varepsilon)G(\varepsilon)\right] = \lambda, \quad \text{(D18)}$$

$$\frac{2}{\pi}\int_{-\Lambda_0}^{E_F} d\varepsilon\,{\rm Im}\,G(\varepsilon) = r^2-1. \quad \text{(D19)}$$

Equations (D18), (D19), and (D11) constitute a closed set from which the parameters λ and r can be self-consistently calculated.

After λ and r are determined, the impurity level ε_d is renormalized to the Kondo resonance at ε_K in the impurity spectral density $A(\varepsilon) \equiv -\frac{1}{\pi}{\rm Im}G(\varepsilon)$, with the Kondo temperature defined as

$$T_K = \sqrt{(\varepsilon_K-E_F)^2 + r^4\Gamma^2(\varepsilon_K)}, \quad \text{(D20)}$$

where ε_K is the pole of the impurity Green function $G(\varepsilon)$, which can be determined from the equation

$$\varepsilon_K - (\varepsilon_d+\lambda) - r^2\,{\rm Re}\,\Sigma(\varepsilon_K) = 0. \quad \text{(D21)}$$

When the impurity level is deep below E_F (the regime where the slave-boson mean-field theory is valid), the electron number $1-r^2$ in the impurity is almost 1 and the hole number r^2 is very close to zero. Therefore, we can always approximate

$$\varepsilon_K \simeq \varepsilon_d + \lambda. \quad \text{(D22)}$$

The slave-boson mean-field theory neglects the dynamics of the boson fields and hence charge fluctuations in the impurity. But it correctly captures spin fluctuations. Therefore it is suitable for studying the Kondo problem of a very deep impurity level, where charge fluctuations are frozen out. In this regime, the mean-field approximation can give a faithful description of the strong-coupling Kondo fixed point, resulting in a local Fermi-liquid behavior at zero temperature. Note that the mean-field equations derived here are quite general, having no restrictions in the bath density of states except its spin independence. For a flat band of normal metal, e.g., $\widetilde{\rho}(\varepsilon) = \widetilde{\rho}_0$, the saddle-point equation (D18) is analytically integrable, giving rise to the well-known Kondo temperature $T_K^0 = \Lambda_0\exp[(\varepsilon_d-E_F)/(2V_0^2\widetilde{\rho}_0)]$. For the nanotube bath considered in this paper, $\widetilde{\rho}(\varepsilon)$ is energy dependent, and more importantly, is gapped around E_F. In this case, Eq. (D18) has a phase transition. At the critical point $\varepsilon_d = \varepsilon_{dc}$, the Kondo temperature must vanish $T_K = 0$, requiring

$$r = 0, \quad \lambda = E_F - \varepsilon_{dc}. \quad \text{(D23)}$$

Substituting Eq. (D23) together with $\varepsilon_d = \varepsilon_{dc}$ into Eq. (D18), we obtain the following critical equation (after some calculations):

$$\varepsilon_{dc} - E_F = \frac{1}{\pi}\int_{-\Lambda_0}^{E_F} d\varepsilon\frac{\Gamma(\varepsilon)}{\varepsilon-E_F} + \frac{1}{\pi}\int_{E_F}^{\Lambda_0} d\varepsilon\frac{\Gamma(\varepsilon)}{E_F-\varepsilon}. \quad \text{(D24)}$$

Note that the critical value of the impurity level ε_{dc} is always below E_F. For $\varepsilon_{dc} < \varepsilon_d < E_F$, the closed set of mean-field equations has a Kondo solution, and the impurity can reach the strong-coupling fixed point. On the other hand, when $\varepsilon_d < \varepsilon_{dc} < E_F$, the mean-field equations break down, having no self-consistent solutions. This means that the impurity remains an unscreened local moment. Equation (D24) also indicates that ε_{dc} is finite only if $\widetilde{\rho}(E_F) = 0$, otherwise $\varepsilon_{dc} \to -\infty$, signaling a robust Kondo state without phase transition to the local-moment phase.

APPENDIX E: PHASE DIAGRAMS FOR *S*- AND *C*-SITE IMPURITIES IN THE ($\widetilde{\varepsilon}_d$, E_F) PLANE

As shown in Fig. 5, the Kondo and LM phases of S or C impurities are also bounded by an arched borderline, showing features qualitatively same with T-site adatoms [see Fig. 2(a) in the main text]. For example, the boundary is p-h symmetric for armchair nanotubes but becomes p-h asymmetric for nonarmchair nanotubes. The minimal radius R_1 derived in the main text for accessing the maximal p-h asymmetry also applies to this case. This is because $\widetilde{\rho}_{\rm sc}(\varepsilon)$ and $\widetilde{\rho}_{\rm T}(\varepsilon)$ share the same gap structure which determines the main structure of phase diagrams in the ($\widetilde{\varepsilon}_d$, E_F) plane. $\widetilde{\rho}_{\rm sc}(\varepsilon)$ and $\widetilde{\rho}_{\rm T}(\varepsilon)$ scale differently only outside the gap region due to the quantum interference effect.

The effect of quantum interference is mainly reflected (i) in the R dependence of the boundary (see Fig. 1), (ii) in the

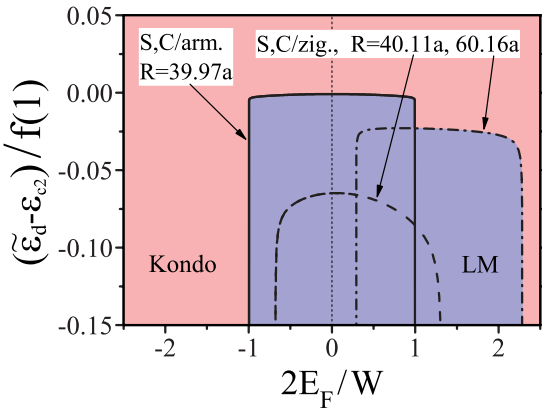

FIG. 5. (Color online) Phase diagrams for substitutional dopants or C-site adatoms in armchair and zigzag nanotubes in the ($\widetilde{\varepsilon}_d$, E_F) plane. The parameters used here are the same as in Fig. 2(a).

fact that the arched LM region of S or C impurities are much sharper than T adatoms [compare Fig. 2(a) with Fig. 5], and (iii) in the fact that for realistic nanotube parameters, the Kondo boundary of S or C impurities, $\widetilde{\varepsilon}_{dc}$, is always much shallower than the boundary of T adatoms, signaling the reduction of the Kondo regime by interference.

[1] J.-C. Charlier, X. Blase, and S. Roche, Rev. Mod. Phys. **79**, 677 (2007).

[2] J. Nygård, D. H. Cobden, and P. E. Lindelof, Nature (London) **408**, 342 (2000); M. Pustilnik, Y. Avishai, and K. Kikoin, Phys. Rev. Lett. **84**, 1756 (2000); J. Paaske, A. Rosch, P. Wölfle, N. Mason, C. M. Marcus, and J. Nygård, Nat. Phys. **2**, 460 (2006).

[3] T. Delattre, C. Feuillet-Palma, L. G. Herrmann, P. Morfin, J.-M. Berroir, G. Fève, B. Placais, D. C. Glattli, M.-S. Choi, C. Mora, and T. Kontos, Nat. Phys. **5**, 208 (2009); P. Vitushinsky, A. A. Clerk, and K. Le Hur, Phys. Rev. Lett. **100**, 036603 (2008); J. Basset, A. Yu. Kasumov, C. P. Moca, G. Zaránd, P. Simon, H. Bouchiat, and R. Deblock, *ibid.* **108**, 046802 (2012).

[4] M.-S. Choi, R. López, and R. Aguado, Phys. Rev. Lett. **95**, 067204 (2005); P. Jarillo-Herrero, J. Kong, H. S. J. van der Zant, C. Dekker, L. P. Kouwenhoven, and S. De Franceschi, Nature (London) **434**, 484 (2005); A. Makarovski, J. Liu, and G. Finkelstein, Phys. Rev. Lett. **99**, 066801 (2007); F. B. Anders, D. E. Logan, M. R. Galpin, and G. Finkelstein, *ibid.* **100**, 086809 (2008).

[5] J. R. Hauptmann, J. Paaske, and P. E. Lindelof, Nat. Phys. **4**, 373 (2008); M. Gaass, A. K. Hüttel, K. Kang, I. Weymann, J. von Delft, and Ch. Strunk, Phys. Rev. Lett. **107**, 176808 (2011).

[6] M. R. Buitelaar, T. Nussbaumer, and C. Schönenberger, Phys. Rev. Lett. **89**, 256801 (2002); A. Eichler, M. Weiss, S. Oberholzer, C. Schönenberger, A. Levy Yeyati, J. C. Cuevas, A. Martín-Rodero, *ibid.* **99**, 126602 (2007); J. S. Lim, R. López, and R. Aguado, *ibid.* **107**, 196801 (2011).

[7] T. W. Odom, J.-L. Huang, C. L. Cheung, and C. M. Lieber, Science **290**, 1549 (2000).

[8] D. P. Clougherty, Phys. Rev. Lett. **90**, 035507 (2003).

[9] G. A. Fiete, G. Zarand, B. I. Halperin, and Y. Oreg, Phys. Rev. B **66**, 024431 (2002).

[10] P. P. Baruselli, A. Smogunov, M. Fabrizio, and E. Tosatti, Phys. Rev. Lett. **108**, 206807 (2012).

[11] A. C. Hewson, *The Kondo Problem to Heavy Fermions* (Cambridge University Press, Cambridge, 1993).

[12] F. Kuemmeth, S. Ilani, D. C. Ralph, and P. L. McEuen, Nature (London) **452**, 448 (2008); H. O. H. Churchill, F. Kuemmeth, J. W. Harlow, A. J. Bestwick, E. I. Rashba, K. Flensberg, C. H. Stwertka, T. Taychatanapat, S. K. Watson, and C. M. Marcus, Phys. Rev. Lett. **102**, 166802 (2009); S. H. Jhang, M. Marganska, Y. Skourski, D. Preusche, B. Witkamp, M. Grifoni, H. van der Zant, J. Wosnitza, and C. Strunk, Phys. Rev. B **82**, 041404(R) (2010); T. S. Jespersen, K. Grove-Rasmussen, J. Paaske, K. Muraki, T. Fujisawa, J. Nygård, and K. Flensberg, Nat. Phys. **7**, 348 (2011).

[13] D. Huertas-Hernando, F. Guinea, and A. Brataas, Phys. Rev. B **74**, 155426 (2006); D. V. Bulaev, B. Trauzettel, and D. Loss, *ibid.* **77**, 235301 (2008); L. Chico, M. P. López-Sancho, and M. C. Muñoz, *ibid.* **79**, 235423 (2009); J.-S. Jeong and H.-W. Lee, *ibid.* **80**, 075409 (2009); S. Weiss, E. I. Rashba, F. Kuemmeth, H. O. H. Churchill, and K. Flensberg, *ibid.* **82**, 165427 (2010).

[14] J. Klinovaja, M. J. Schmidt, B. Braunecker, and D. Loss, Phys. Rev. B **84**, 085452 (2011).

[15] M. del Valle, M. Margańska, and M. Grifoni, Phys. Rev. B **84**, 165427 (2011); W. Izumida, K. Sato, and R. Saito, J. Phys. Soc. Jpn. **78**, 074707 (2009).

[16] R. Bulla, T. A. Costi, and T. Pruschke, Rev. Mod. Phys. **80**, 395 (2008).

[17] J. R. Schrieffer and P. A. Wolff, Phys. Rev. **149**, 491 (1966).

[18] L. Fritz and M. Vojta, Phys. Rev. B **70**, 214427 (2004).

[19] K. Chen and C. Jayaprakash, Phys. Rev. B **57**, 5225 (1998); C. P. Moca and A. Roman, *ibid.* **81**, 235106 (2010).

[20] P. W. Anderson, J. Phys. C **3**, 2436 (1970); F. D. M. Haldane, Phys. Rev. Lett. **40**, 416 (1978).

[21] P. Coleman, Phys. Rev. B **29**, 3035 (1984); **35**, 5072 (1987); N. Read and D. M. Newns, J. Phys. C **16**, L1055 (1983).

[22] R. Saito, G. Dresselhaus, and M. S. Dresselhaus, *Physical Properties of Carbon Nanotubes* (Imperial College Press, London, 1998).

[23] D. Tománek and M. A. Schluter, Phys. Rev. Lett. **67**, 2331 (1991); J. W. Mintmire and C. T. White, Carbon **33**, 893 (1995).